4 May 1979, Volume 204, Number 4392 **SCIENCE**

Laser Annealing of Ion-Implanted Semiconductors

C. W. White, J. Narayan, R. T. Young

Impurities can be implanted in the near-surface region of solids by a process in which the impurity ions are accelerated in an electrostatic field to a desired energy and then made to impinge on the solid targets. This process, known as ion implantation, has made a significant impact on the electronics industry, where it is used to dope semiconductors is often accompanied by undesirable consequences such as precipitation of dopants in the implanted region, degradation of certain electrical properties, decomposition of the substrate in the case of compound semiconductors, and usually only partial removal of lattice damage in the implanted layer.

Recently, interest (*1*) has been gener-

Summary. The physical and electrical properties of ion-implanted silicon annealed with high-powered laser radiation are described. Particular emphasis is placed on the comparison of materials properties that can be achieved with laser annealing to those which can be achieved by conventional thermal annealing. Applications of these techniques to the fabrication of high-efficiency solar cells, and potential applications of this new technique to other materials areas are discussed.

in a controlled and reproducible manner for p-n junction formation in device processing. A major problem with ion implantation, however, is that damage is produced in the crystal lattice as the implanted ions lose energy and ultimately come to rest in the solid. After implantation of semiconductors, the near-surface region of the sample is heavily damaged and may even be amorphous; in addition, the implanted dopants are not electrically active because they do not occupy substitutional sites in the crystal lattice. For most applications it is necessary to anneal the solid in order to remove the displacement damage and to activate the implanted ions electrically. Conventionally, this has been done by heating the entire sample to temperatures of several hundred degrees for 30 minutes or longer, but thermal annealing

ated in the possibility of using high-powered laser radiation as a more effective means for annealing ion-implanted materials. Laser annealing can be accomplished simply by illuminating the implanted material with laser radiation of the appropriate wavelengths, energy densities, and pulse durations. Pioneering work by Soviet scientists, which established the laser annealing phenomenon (*2-4*), has stimulated research activities (*5-33*) at many laboratories throughout the world, because laser annealing appears to offer distinct advantages over thermal annealing for processing implanted materials. One great advantage is that the laser light is heavily absorbed in a thin surface layer a few hundred to a few thousand angstroms deep in the solid. This produces the very high temperatures (even melting) in the implanted region which are necessary for annealing the lattice damage; yet, the absorbed photon energy is insufficient to raise the temperature of the undamaged substrate significantly above ambient, and hence the deleterious effects of high temperatures in this region are circumvented. Another advantage for some applications is that laser annealing can be carried out in air because the surface region subjected to high temperatures cools so rapidly that introduction of significant amounts of impurities from the atmosphere is minimized. This should be a particularly attractive feature for highly automated device fabrication. A third, and potentially very important, advantage of laser annealing is that it enables highly localized annealing to be performed simply by focusing the incident laser light to the desired dimensions (*21*). This may permit the "writing" of regions of localized electrical activity on an ion-implanted wafer and could have profound implications for device processing.

In this article, we review results of work performed at Oak Ridge National Laboratory (ORNL) on the characterization of ion-implanted silicon annealed by radiation from pulsed ruby lasers. We place particular emphasis on the comparison of laser annealing with conventional thermal annealing, and discuss the major results of a wide variety of experimental and theoretical studies at ORNL. More details of this work (*5-19*) and of the work conducted at other laboratories (*20-33*) have been published elsewhere.

Our results to date show that laser annealing can lead to complete removal of displacement damage in ion-implanted silicon, with no degradation of the minority carrier lifetime in the substrate. Dopant spatial profiles can be considerably broadened by pulsed laser annealing, and this broadening has been correlated with the results of calculations which strongly indicate that the annealing mechanism involves melting of the crystal in the near-surface region, dopant

The authors are research staff members in the Solid State Division of the Oak Ridge National Laboratory, Oak Ridge, Tennessee 37830.

0036-8075/79/0504-0461$02.00/0 Copyright © 1979 AAAS

diffusion in the molten state, and, subsequently, liquid phase epitaxial regrowth from the underlying substrate. Implanted dopants are found to occupy substitutional sites in the silicon lattice after annealing, even when the dopant concentration far exceeds the limits of equilibrium solid solubility. A unique one-dimensional expansion or contraction of the lattice in the implanted region in a direction perpendicular to the surface can be produced by laser annealing. We present here results of the application of laser annealing to the fabrication of high-efficiency solar cells, and describe briefly some studies of laser-induced diffusion of surface-deposited (rather than ion-implanted) dopants into semiconductors for formation of p-n junctions. We conclude by indicating other areas where laser annealing and laser-induced diffusion may find application.

Choice of Lasers and Sample Preparation

The lasers used thus far to perform annealing have been commercially available ones of both the continuous wave (CW) and pulsed type. Most of the work has been done with *Q*-switched ruby (*2, 5, 25*) and neodymium : yttrium aluminum garnet (Nd : YAG) lasers (*3, 20*), and CW argon ion lasers operated in a scanning mode (*4, 23, 32, 33*). A *Q*-switched laser emits a pulse of energetic photons in a time interval that can be varied between 20 and 100 nsec (1 nanosecond = 10^{-9} second), and annealing can be achieved by choosing the proper photon energy density and pulse duration. A CW laser emits a continuous wave of photons, and appropriate annealing conditions can be achieved by varying the power output of the laser or the rate at which the photon beam is scanned across the sample. Both types of lasers have been shown to produce high-quality annealing, but the mechanisms giving rise to the annealing and some of the characteristics of the laser-annealed material can be different. Most of the results reported in this article were obtained by using the multimode output of a *Q*-switched ruby laser with a pulse duration time of approximately 50 nsec and an energy density that could be varied between 0.6 and 3.0 joules per square centimeter. The beam diameter was 1.6 cm, and this could be expanded further by a defocusing lens. Most samples were annealed by a single laser pulse, but larger samples required a few overlapping pulses. Laser energy densities of 1.5 to 1.7 J/cm^2 were generally used in this work because this range is significantly above the threshold energy for annealing (roughly 1 J/cm^2 for our implantation conditions) but below the threshold density for surface damage of 2.0 to 3.0 J/cm^2, depend-

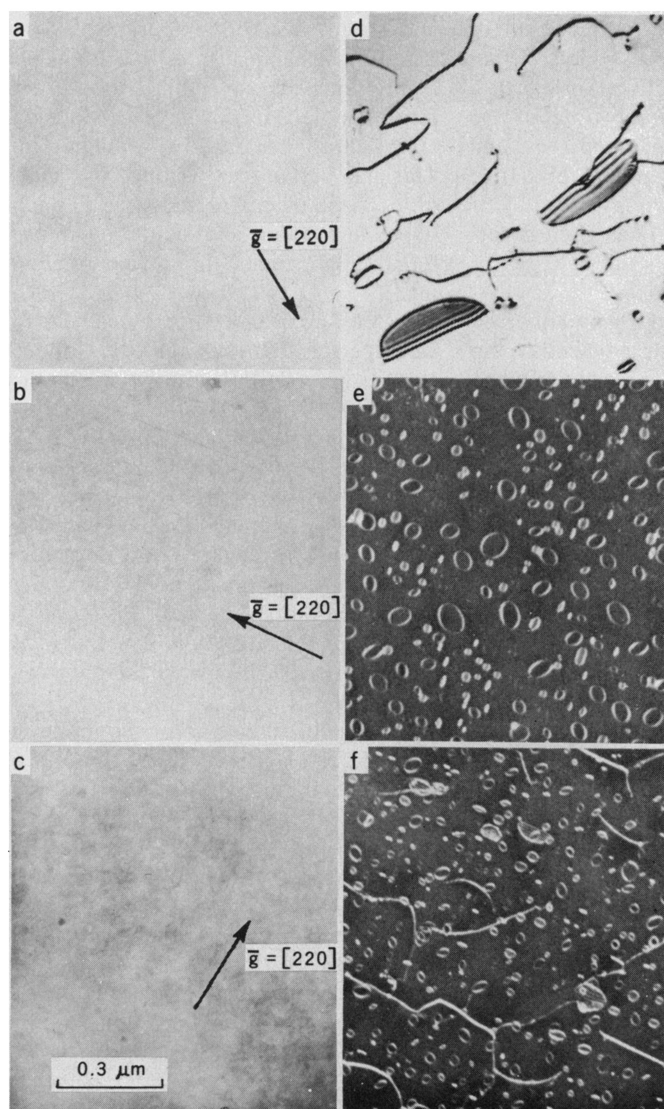

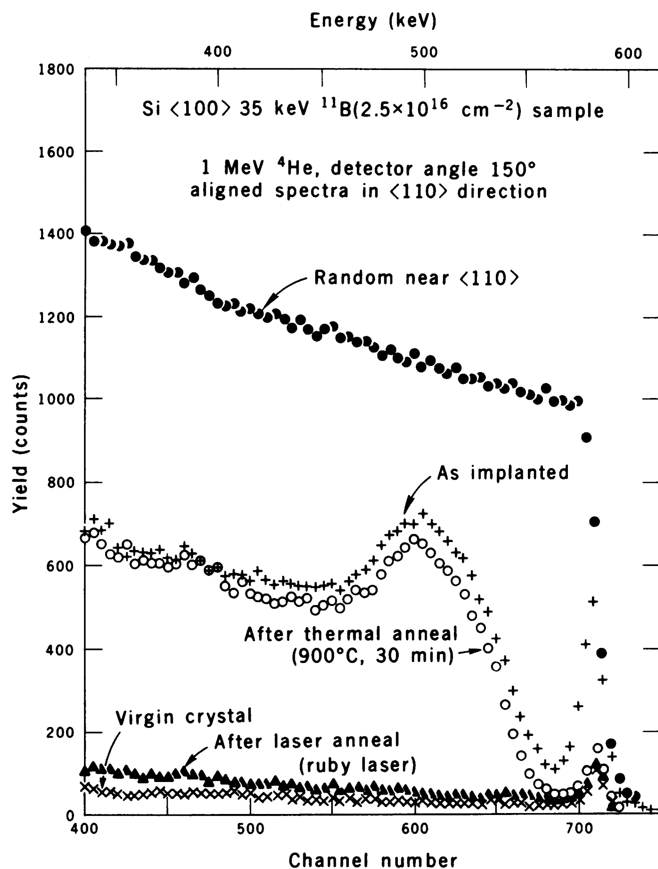

Fig. 1 (left). Transmission electron micrographs comparing (a to c) laser- and (d to f) thermally annealed ion-implanted silicon (001) orientation. Implanted species, energy, dose, projected range (*39*), and range straggling (*39*) were: (a and d) ^{11}B (35 keV, 3 × 10^{15} cm^{-2}, 1100 Å, 420 Å); (b and e) ^{31}P (80 keV, 1 × 10^{15} cm^{-2}, 1000 Å, 400 Å); (c and f) ^{75}As (100 keV, 1 × 10^{16} cm^{-2}, 560 Å, 200 Å). The boron and phosphorus samples were thermally annealed at 1100°C for 30 minutes and the arsenic sample at 900°C for 30 minutes. Micrographs (a) through (d) were taken in bright field, and (e) and (f) in dark field. The symbol g is the diffraction vector. Fig. 2 (right). Backscattered ^{4}He energy spectra for virgin silicon crystal and ^{11}B-implanted crystals (as implanted, thermally annealed, laser annealed). The incident beam was aligned along the [110] axial direction.

ing on the pulse duration time. Ruby lasers are well suited for research on laser annealing of semiconductors such as silicon and gallium arsenide, because the 0.694-micrometer wavelength of the radiation is sufficient to excite electrons from the valence to the conduction band and the absorption coefficients of the materials are high. Thus the radiation is heavily absorbed in the first few thousand angstroms of the solid and very rapidly raises the temperature of the implanted region to the desired level. By utilizing the short pulse duration times of the *Q*-switched mode, the total energy that is transferred to the bulk of the crystal by thermal conduction during the laser pulse is minimized.

For the work described here, semiconductor-grade, single-crystal silicon samples cut with a (100) orientation were used as substrates, and the implanted ions include boron, phosphorus, arsenic, and antimony, since these are the most important dopants in silicon. The dose range for ion implantation extended from 10^{14} to 10^{17} ions per square centimeter; this covers the range of interest in device fabrication and extends to dopant concentrations in the implanted region which greatly exceed the limit of solid solubility. Implants were done at room temperature under high vacuum conditions (2×10^{-8} torr) at energies ranging from 35 to 100 kiloelectron volts. Unless otherwise stated, laser annealing was accomplished with 1.5 J/cm², 60-nsec pulses.

Removal of Lattice Damage

A direct comparison of the effects of laser and thermal annealing is shown by the transmission electron micrographs of Fig. 1. (*5–8*). Transmission electron microscopy concerns the formation of highly magnified images with the use of electrons that have been transmitted through thin sections of a solid. Contrast in the image arises from differences in the intensity of electrons contributing to the image as a result of local variations in electron scattering. For crystalline solids, electron scattering takes the form of one or more diffracted beams whose intensities are affected by defects in the crystal structure, and images of these defects can be formed with either the direct transmitted beam (bright field) or a diffracted beam (dark field). In Fig. 1, the electron microscope was used to examine the region extending from the surface down to a depth of approximately 5000 Å, which includes both the range of the implanted species as well as the region in which damage in the substrate lattice was produced by the implantation process. Figure 1, a to c, shows that no damage remains in the laser-annealed specimens in the form of dislocations, stacking faults, or dislocation loops, down to the resolution of the microscope which was approximately 10 Å. Electron diffraction patterns from these laser-annealed crystals show that the implanted region has the same (001) orientation as the substrate. The fact that there are no irregularities in the electron diffraction patterns is another indication of the perfection of the lattice. Even after subsequent heating of the laser-annealed crystals to temperatures of 900°C there was no observable agglomeration of point defects or clusters (*7*), showing that residual damage after laser annealing must be very small, if there is any. By contrast, after thermal annealing (Fig. 1, d to f), significant damage remains in the form of dislocation loops. The conclusion from these observations is that pulsed laser annealing is much more effective in removing displacement damage and restoring crystalline order than is conventional thermal annealing.

Another method that is used to measure lattice damage is the Rutherford ion-backscattering and ion-channeling technique. Rutherford backscattering is the classical Coulomb scattering of incident ions from atoms in the solid. Channeling refers to the reduced scattering probability that occurs when the incident beam is aligned along the open channels that exist between rows and planes of atoms in the solid. If atoms are displaced from their normal lattice position, this can be detected by the increase in scattering yield with the beam aligned along a channeling direction.

Figure 2 shows Rutherford backscattering spectra obtained from boron-implanted crystals in the arsenic-implanted, thermally annealed, and laser-annealed conditions compared with similar results obtained from a virgin (un-

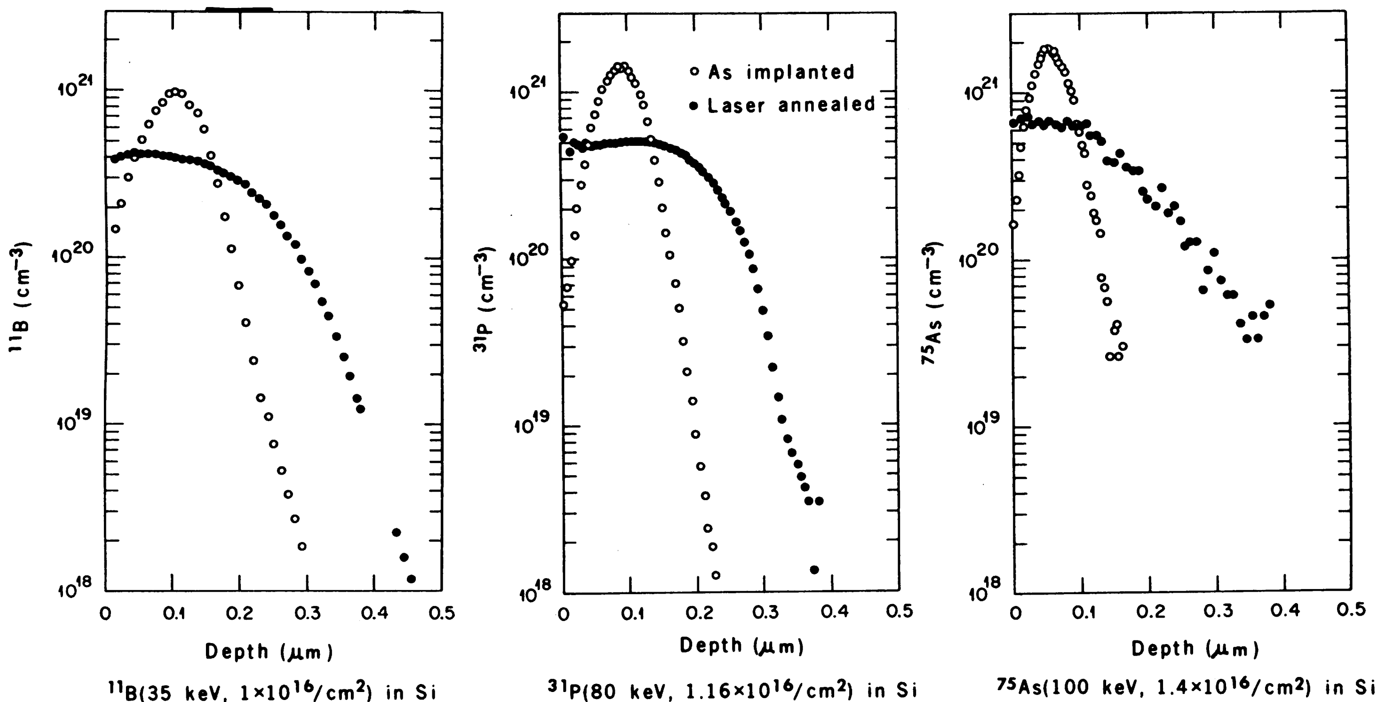

Fig. 3. Dopant concentration profiles of ^{11}B-, ^{31}P-, and ^{75}As-implanted silicon. Profiles were measured before and after laser annealing.

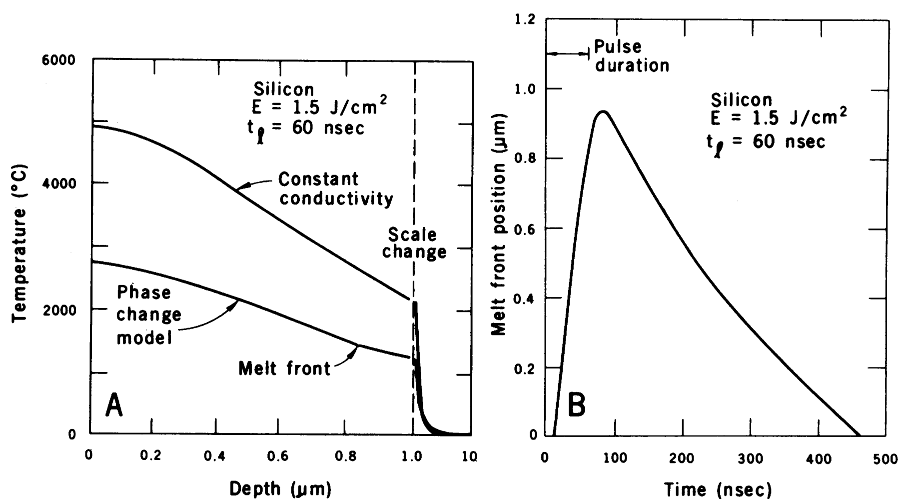

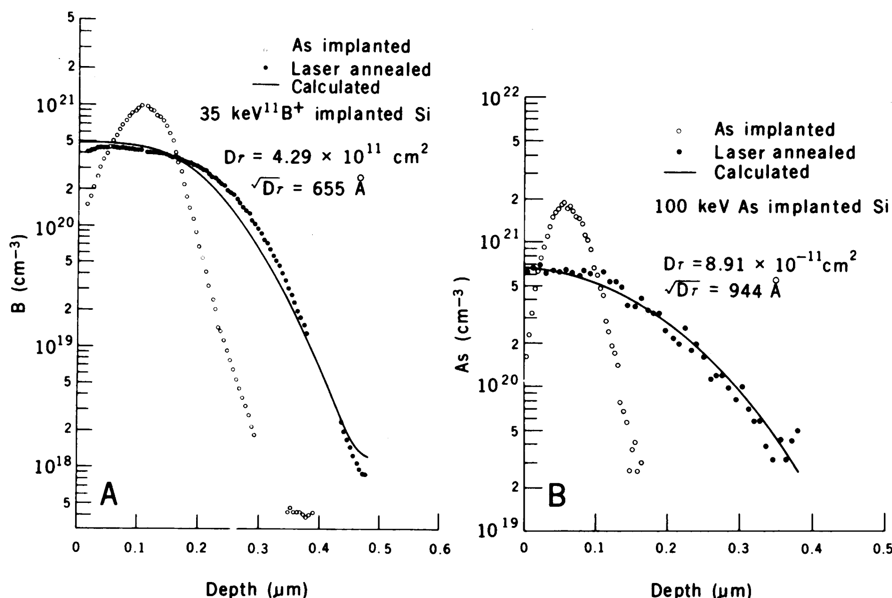

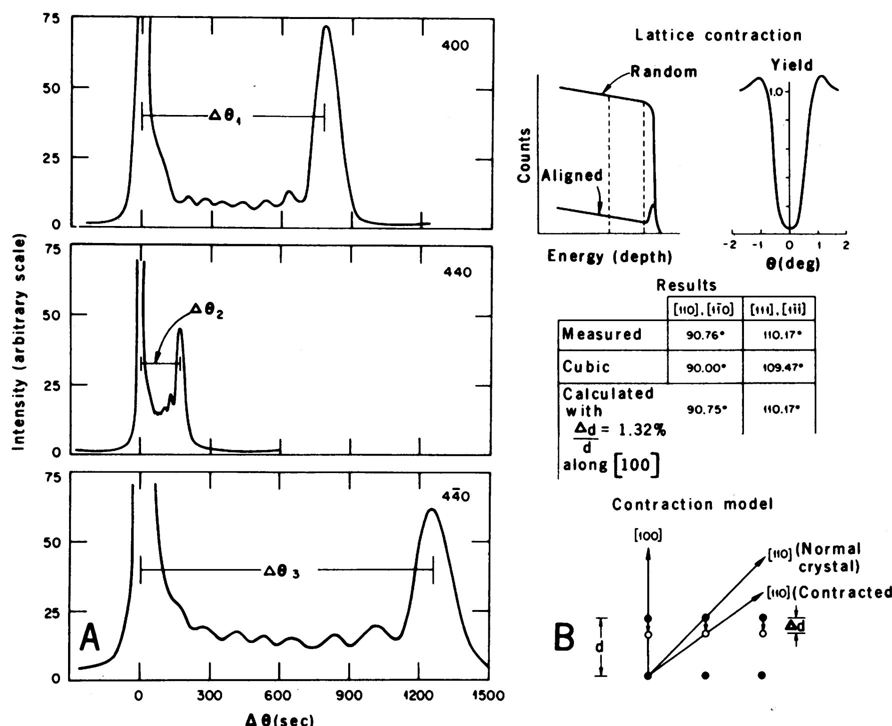

implanted and unannealed) crystal (*5*). These measurements were obtained by using a 1-megaelectron volt collimated beam of $^4He^+$ ions with the beam aligned along the [110] axial direction of the various crystals. The arsenic-implanted spectrum has a broad peak arising from the damage introduced into the silicon lattice by the implanted boron ions. This result shows that the arsenic-implanted crystal is heavily damaged, although not amorphous, because the aligned yield approaches but does not reach the yield obtained with the beam incident along a random direction. As shown in Fig. 2, thermal annealing at 900°C for 30 minutes has little effect on the spectrum, and massive damage still remains in the crystal. After laser annealing, however, there is a dramatic change in the aligned spectrum such that the yield is only slightly greater than that obtained from the virgin crystal, and there is no remaining evidence of any damage in the silicon lattice. These measurements show directly that the long-range, crystalline order has been restored to the implanted region by laser annealing, a conclusion which is in good agreement with the transmission electron microscope results. Channeling studies in the cases of phosphorus-, arsenic-, and antimony-implanted silicon crystals (*9*) that were laser annealed in the same manner also show complete removal of lattice damage.

Dopant Profile Changes During Laser Annealing

Figure 3 shows the effects of pulsed laser annealing on dopant concentration profiles (*10, 11*) for the case of boron, phosphorus, and arsenic implanted into silicon at doses of $\sim 1 \times 10^{16}$ per square centimeter. Profiles for boron and phosphorus were measured by secondary ion mass spectroscopy and the profile for arsenic was measured by Rutherford backscattering. In each case, the laser anneal caused a substantial redistribution of the centration in the liquid at the moving liq-

Fig. 4 (top). (A) Calculated temperature distribution in silicon at the termination of the laser pulse. (B) Calculated melt front penetration in silicon during and after the laser pulse; t_ℓ, pulse duration time. Fig. 5 (center). (A) Comparison in experimental and calculated ^{11}B profiles in silicon after laser annealing. (B) Comparison of experimental and calculated arsenic-75 profiles in silicon after laser annealing. Fig. 6 (bottom). (A) X-ray Bragg reflection profiles from ^{11}B (35 keV, 1×10^{16} per square centimeter) implanted, laser-annealed silicon. (B) Axial ion-channeling results on lattice contraction in ^{11}B (35 keV, 2.5×10^{16} per square centimeter) implanted, laser-annealed silicon.

dopant such that the concentration was almost uniform from the surface down to a depth of 1000 to 2000 Å. Redistribution of these dopants by pulsed laser annealing cannot be explained by diffusion in the solid because the time for diffusion is too short. Recent calculations (*12*), however, give convincing evidence that the crystal is melted by the laser to a depth somewhat greater than that of the implanted profile, and since diffusion coefficients in molten silicon (*34*) are almost seven orders of magnitude higher than those in the solid at temperatures near the melting point (*35*, pp. 38, 39), the observed data can be readily understood. The most significant results of these calculations are summarized in Figs. 4 and 5. Figure 4A shows calculated temperature profiles at the termination of the laser pulse. The upper curve is a typical temperature distribution obtained from an analytical solution of the one-dimensional heat conduction equation when melting does not occur and the thermal conductivity and specific heat are assumed to be constant with temperature. The lower curve of Fig. 4A was obtained from numerical solution of the same equation, which had been generalized to allow for the possibility of a phase change (melting) and for temperature-dependent thermal conductivity and specific heat. As predicted by this curve, at the termination of the laser pulse the crystal was melted to a depth of almost 0.85 μm.

From a series of curves such as the lower one in Fig. 4A, the position of the melt front as a function of time during and after the laser pulse can be determined; typical results are shown in Fig. 4B. The melt front very rapidly penetrates to a depth of about 0.95 μm in the solid, before receding back to the surface with an average velocity of approximately 270 cm/sec. While this occurs, a region that is almost 5000 Å thick remains in the molten state for a few hundred nanoseconds during which time the dopants can diffuse over significant distances in the liquid because diffusion coefficients are so much higher than in the solid. In Fig. 5, A and B, the experimental profiles in Fig. 3 for boron and arsenic after laser annealing are compared to profiles calculated with the assumption that the implanted ions diffuse in liquid silicon; the agreement is very good. From the calculated profiles, the square of the diffusion length ($D\tau$) can be obtained, and it is indicated on the figures for each species. Using these results and literature values for the diffusion coefficients in liquid silicon (*34*), one can extract values for the diffusion time (τ). The resulting times of 180 nsec for boron and 270 nsec for arsenic are in good agreement with the melt front predictions of Fig. 4B.

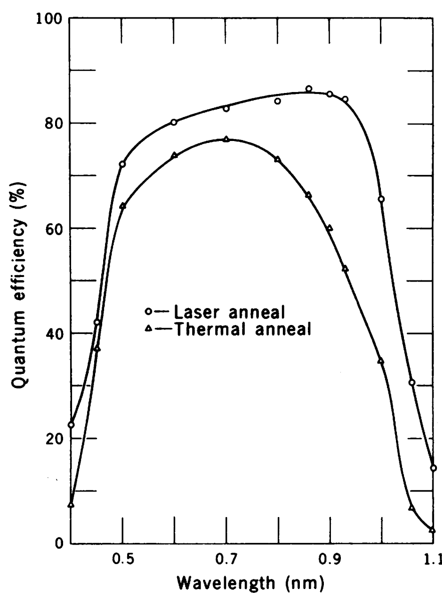

Fig. 7. Quantum response of laser and thermally annealed solar cells. The charged carriers collected per incident photon are plotted as a function of the wavelength of the incident light. The size of the cells in each case was 1 by 2 cm, and the laser-annealed cell was processed by using two overlapping laser pulses.

If one compares the calculations with the experimental results, the pulsed laser annealing process for typical conditions can be pictured as follows. The incident laser light melts the crystal to a depth somewhat greater than that of the implanted profile. The melted region then recrystallizes from the underlying substrate by liquid phase epitaxial regrowth, resulting in defect-free single crystal material with dopants in substitutional sites in the silicon lattice. During the time the implanted region is molten, dopants can diffuse in the liquid where diffusion rates are much higher than in the solid. Similar conclusions regarding melting of the sample in the case of *Q*-switched laser annealing have been reported by others (*21, 28, 30*).

Annealing can be achieved in the absence of significant dopant redistribution by using scanned CW lasers (*23, 31–33*). In that case, the absorbed laser light heats the implanted region to temperatures near the melting point for time periods (~10^{-3} second) sufficient for annealing to take place by solid phase reactions (solid phase epitaxial regrowth). The time available for annealing with *Q*-switched lasers is too short for damaged layers several thousand angstroms in thickness to be annealed with a single pulse by solid phase epitaxial regrowth. Consequently, melting followed by liquid phase epitaxial regrowth may be essential with the short-pulse duration times of *Q*-switched lasers. Melting will inevitably be accompanied by some dopant redistribution.

Lattice Modifications Induced by Laser Annealing

Significant modifications can take place in the implanted reigon of the silicon lattice as a consequence of laser annealing. One change involves the substitution of implanted dopant atoms for silicon atoms at normal positions in the lattice (substitutional lattice sites). The location of implanted dopants such as arsenic and antimony in the lattice after laser annealing has been determined by means of ion-backscattering and ion-channeling techniques (*9*). Both aligned axial channeling spectra and detailed angular scans across the major axial directions were used to determine the lattice location. Implanting arsenic and antimony (100 keV energy) into single crystal silicon at doses in excess of 10^{15} per square centimeter creates an amorphous region to a depth of ~1500 Å. Annealing with a single laser pulse completely restores single crystal order to the implanted region and is accompanied by incorporation of the dopants into substitutional sites in the silicon lattice. For all antimony implant doses from 10^{15} to 1.5×10^{16} per square centimeter, the substitutional fraction after laser annealing measured 98 to 99 percent. [By contrast, the highest substitutional fractions that have been reported after thermal annealing are about 90 percent (*36*).] In the case of arsenic-75 implants, the substitutional fractions were equally high, being in the 98 to 99 percent range for implant doses up to 5×10^{16} per square centimeter.

The results of these ion backscattering and channeling measurements clearly show that the implanted dopant can be incorporated into substitutional lattice sites at concentrations far exceeding the equilibrium solid solubility limit. The antimony concentration in substitutional lattice sites in the implanted region after laser annealing has been found to be as high as 1.5×10^{21} per cubic centimeter, while the solid solubility limit (*35*, p. 45) at the melting point is 4×10^{19} per cubic centimeter. Exceeding the limit of solid solubility by pulsed laser annealing apparently is related to the very short time associated with the annealing process. During liquid-phase epitaxial regrowth, dopants are incorporated into the solid at concentrations determined by the concentration in the liquid at the moving liq-

uid-solid interface. Regrowth takes place in a few hundred nanoseconds and the regrown region then rapidly cools toward ambient temperatures in a few microseconds. This time is too short for precipitation to occur in the solid because solid-phase diffusivities (*35*, pp. 38, 39) are too low. These results therefore represent the application of laser annealing to the fabrication of materials with properties that could not be achieved by conventional thermal processing. The excess concentration above the solubility limit is a supersaturated or metastable condition, but these systems are quite stable at temperatures below approximately 600°C. However, precipitation will occur if the supersaturated laser-annealed crystals are heated subsequently to higher temperatures (*7, 8*).

The silicon lattice also undergoes a significant one-dimensional contraction or expansion in the implanted region during laser annealing (*13*). The physical size (ionic radius) of the dopant atom relative to that of the silicon atom it displaces in the lattice determines whether the lattice will expand or contract. For example, the atomic radii of boron and phosphorus are less than that of silicon, and these ions produce a net contraction in the implanted region; antimony, which is larger than silicon, causes the lattice to expand; and arsenic, which is very nearly equal in size to silicon, produces no measurable change.

The lattice contraction (or expansion) occurs in one dimension in a direction normal to the surface (*13*). Both the direction and magnitude have been measured by x-ray diffraction and ion-channeling techniques. X-ray Bragg reflection profiles for three different reflections from a boron-implanted silicon crystal which has been laser annealed are given in Fig. 6A. They show secondary Bragg peaks at $\Delta\theta_1$, $\Delta\theta_2$, and $\Delta\theta_3$ arising from the implanted region as well as an intense Bragg peak at $\Delta\theta = 0$ from the substrate. From these results, it can be concluded directly that the lattice parameter in the implanted region is different from that of the underlying substrate, and the fact that $\Delta\theta_2$ is not equal to $\Delta\theta_3$ establishes that the lattice contraction is not cubic. Quantitative analysis of the x-ray data shows that the contraction takes place only along the direction normal to the surface, thus producing tetragonal rather than cubic symmetry in the implanted region.

Table 1. Laser-annealed solar cell parameters.

Parameter
V_{oc} (open-circuit voltage) = 570 mV
J_{sc} (short-circuit current) = 35 mA/cm^2
FF (fill factor) = 0.72
Cell efficiency = 14.5 percent
^{11}B [35 keV, 3×10^{15} per square centimeter implanted (001) 5 ohm-cm silicon (Czochralski process)]
Laser annealing = 1.5 J/cm^2, 20 nsec
Antireflection coating: silicon nitride

Similar results have been obtained by using ion-channeling measurements (depicted schematically in Fig. 6B) on crystals implanted with boron to a dose of 2.5×10^{16} per square centimeter. The orientation of the major axial directions in the implanted region relative to the [100] surface normal were determined by the ion-channeling effect. Ions scattered from a depth of less than 2000 Å in the crystal were used to align the axial directions of the crystal with the incoming beam direction. From the boron profile given in Fig. 3 it can be seen that these ions are scattered from a region with relatively uniform boron concentration (and therefore uniform contraction). The measured angles between the [110] and [1$\bar{1}$0], and the [111] and [1$\bar{1}$1] axial directions in the implanted region are tabulated in Fig. 6B along with the angles expected from cubic symmetry. As shown, there is considerable deviation from cubic symmetry. Assuming a one-dimensional contraction along the [100] surface normal and using the x-ray diffraction lattice parameter change as measured from the (400) reflection for the same sample, one finds that the calculated angles between the major axial directions are in excellent agreement with the experimental measurements.

The one-dimensional lattice change produced by laser annealing at these dopant concentrations of approximately one atomic percent is a unique consequence of laser annealing. In thermal annealing, misfit dislocations that would destroy the one-dimensional nature of the lattice parameter change would be expected at the high dopant concentrations encountered in this work. The time associated with pulsed laser annealing is too short for the development of misfit dislocations which would tend to relieve the strain and destroy the one-dimensional nature of the lattice parameter change. The one-dimensional change occurs through a strict adherence to the underlying crystal planes of the substrate which prevents changes in the plane of the sample and allows lattice parameter changes only along the surface normal.

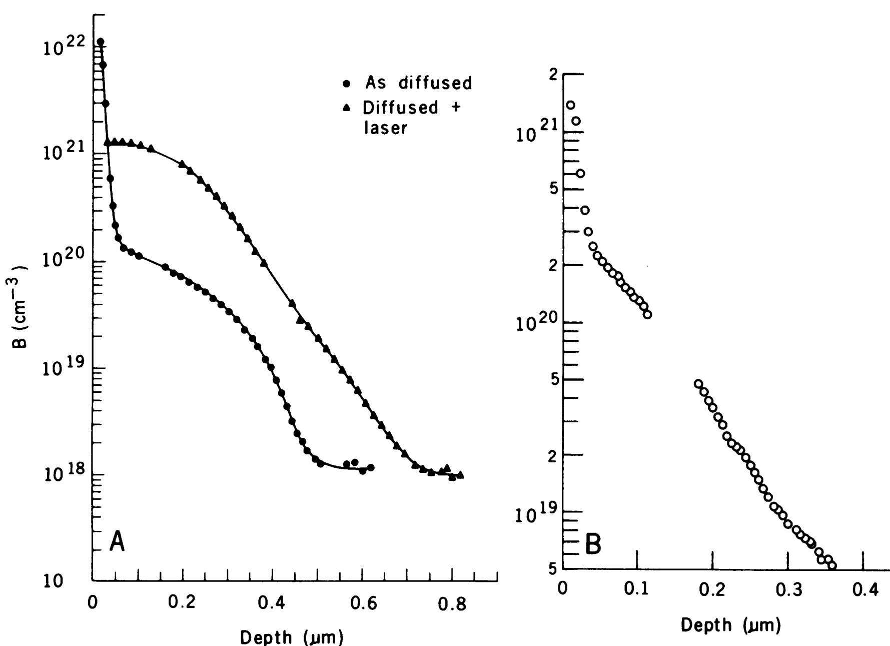

Fig. 8. (A) Concentration profiles of boron-diffused silicon before and after laser irradiation. Diffusion was carried out in a boron diffusion furnace at 1000°C for 10 minutes. The sample was subsequently irradiated with a 1.5 J/cm^2, 60-nsec laser pulse. (B) Concentration profile of boron-deposited, laser-irradiated silicon. For this experiment, boron (~5 μg/cm^2) was evaporated onto the surface of silicon and the sample was subsequently irradiated with a 1.5 J/cm^2, 60-nsec laser pulse.

Improved Electrical Properties for Solar Cells

Laser annealing of ion-implanted silicon yields significant improvements in a number of electrical properties of importance in photovoltaic applications (*5, 9, 14, 15*). One such property is the number of implanted ions which can be electrically activated by substituting them for silicon at normal lattice sites during the

annealing step (*5, 9, 14*). It was shown above that laser annealing is more effective than thermal annealing in bringing about this substitution; hence, it should also be more effective in electrically activating the implanted ions. Measurements of the electrical carrier concentration after laser or thermal annealing for a wide range of implanted doses and atomic species show that this is indeed the case. In fact, since the equilibrium solubility limit cannot be exceeded in thermal annealing, the carrier concentration as a function of implanted dose must saturate, whereas in laser-annealed material it continues to increase linearly up to doses for which the local dopant concentration far exceeds the equilibrium solid solubility limits.

Another electrical property that is superior in diodes made from laser-annealed silicon is the quantum efficiency (carriers collected per incident photon) of response to the solar spectrum (*15*). The absorption coefficient of silicon as a function of photon energy is such that short-wavelength photons (blue region of the spectrum) are absorbed very near the front surface of a sample, whereas the long-wavelength photons (red region) are absorbed in the bulk of the material. This means that the response of a solar cell to light in the blue region is strongly influenced by the properties of the shallow implanted region, and the response to light in the red region is influenced by the properties of the substrate. It was mentioned in the earliest Soviet literature that laser annealing did not degrade the minority carrier lifetime (MCL) in the substrate or base region. The MCL is the average time before recombination of the excess electron-hole pairs created by absorption of incident photons. Charge separation of electron-hole pairs in semiconductors takes place at the p-n junction. Therefore, the MCL of the substrate plays a dominant role in determining the quantum efficiency of solar cells in the long-wavelength spectral region because the electron-hole pairs must diffuse to the junction before recombination occurs.

Extensive measurements (*5*) at ORNL confirm that values of the MCL in the base region before and after laser annealing are very nearly equal, whereas thermal annealing at 1100°C for 30 minutes generally reduces the MCL by a factor of about 10, presumably through the introduction of recombination centers. A comparison of the quantum efficiency of laser and thermally annealed silicon cells is given in Fig. 7, which shows that the response of the laser-annealed cell is superior throughout the entire solar spectrum. The superior response in the red region correlates very well with the retention of a long MCL in the laser-annealed sample. The improvement in the blue region can be attributed to the complete absence in the laser annealed cell of any extended defects which might give rise to trapping and excessive electron-hole recombination.

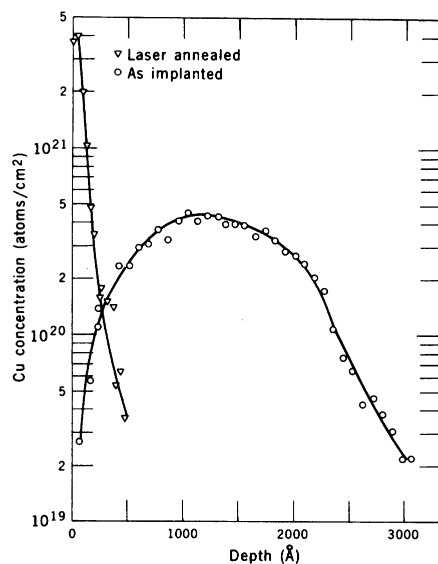

Fig. 9. Concentration profile of $^{63}Cu^{+}$ (150 keV, 6.9 × 10^{15} per square centimeter) implanted ⟨111⟩ silicon before and after laser annealing.

Table 1 summarizes important cell parameters measured for recently fabricated ion-implanted, laser-annealed solar cells. Both the open-circuit voltage V_{oc} and the fill factor, *FF*, of these cells are somewhat lower than values normally obtained from our cells which were doped by standard diffusion techniques. The short-circuit current J_{sc}, however, is the best we have measured on any cell regardless of the fabrication procedures. The cell efficiency (14.5 percent) under AM1 (air mass 1) illumination is almost 50 percent better than we have obtained using conventional (one-step) thermal annealing of boron-implanted silicon and is only slightly lower than the highest value (~ 17.0 percent) reported to date that was obtained by the best boron diffusion techniques (*37*). Significant improvements in ion-implanted, laser-annealed solar cells can be expected by optimizing the laser parameters (energy density, wavelength, pulse duration time), by using lower implant energies, and by the application of back surface fields. Because of the simplicity of the laser-annealing technique and its compatibility with high-speed and low-cost processing, laser annealing should find wide application in the fabrication of high-efficiency solar cells.

Applications of Laser-Induced Melting to Materials Processing

The ultrarapid melting induced by pulsed lasers and subsequent recrystallization of the melted region may also find wide application in materials processing which does not involve ion implantation. Figure 8A shows the effect of laser irradiation on a silicon sample doped with boron by conventional thermal diffusion techniques (*16, 17*). Thermal diffusion results in the formation of a surface layer several hundred angstroms deep containing a very high concentration of electrically inactive dopant atoms in the form of precipitates. After irradiation of the sample with a single laser pulse, the boron profile is significantly redistributed and the boron contained in the precipitates is dissolved and incorporated into solid solution, with an order of magnitude increase in electrical activity. Laser treatment of these diffused crystals has also been found to improve the p-n junction characteristics as determined from measurements on simple diodes.

Laser radiation has been used recently to form large area p-n junctions in silicon by a process of laser-induced diffusion (*18*). For this application, the dopant (boron or aluminum) is evaporated onto the sample surface as a film approximately 100 Å thick and the sample is then irradiated with pulsed laser light. The dopant diffuses into the near surface region of the silicon and becomes electrically active. A spacial profile measured after laser irradiation of boron-deposited silicon is given in Fig. 8B; it shows penetration of boron to a depth of several thousand angstroms in the crystal. The technique of laser-induced diffusion has been applied to the fabrication of solar cells, and efficiencies comparable to those of laser-annealed, ion-implanted cells have been obtained. This type of processing may become especially important for the formation of large-area p-n devices such as solar cells, because it bypasses the ion-implantation step and it does not require heating of the sample to elevated temperatures. This is an attractive method for fabricating a variety of devices which require shallow p-n junctions.

Laser-induced melting may also find application as a method for purifying the near-surface region of materials during processing. Figure 9 shows results (*19*) that were obtained when copper-implanted silicon was laser annealed. After laser annealing, all of the implanted copper was found to be transported to the first few hundred angstroms of the sur-

face where it could be removed by lightly etching the surface. Transport of copper to the surface is apparently the result of its very small segregation coefficient from the liquid. During the process of solidification of the molten silicon, the concentration of copper in the melt builds up until it far exceeds that in the solid. Since the surface is the last region to be solidified (see Fig. 4B), the copper is swept back to the surface and deposited in a thin layer. Since copper acts as a very efficient recombination center in silicon and will seriously degrade the MCL, laser annealing of silicon may offer a very convenient method to reduce the copper concentration in a depth interval equivalent to the melted region. Significant transport of iron to the surface of silicon samples has also been observed after pulsed laser irradiation, and similar results are likely to be found with other impurities whose segregation coefficients in silicon are low.

Conclusions

Laser annealing is superior to thermal annealing as a method for processing ion-implanted silicon. Lattice damage can be removed much more efficiently with laser annealing than with thermal annealing, and dopants can be incorporated into electrically active substitutional lattice sites at concentrations that far exceed equilibrium solid solubility limits. Melting of the surface region followed by liquid phase epitaxial regrowth is the most plausible mechanism for the annealing process. The observed broadening of dopant profiles is consistent with diffusion in the molten state. Substitutional fractions after laser annealing are significantly better than those reported after thermal annealing. Pulsed laser annealing leads to a unique one-dimensional expansion or contraction of the lattice with the absence of misfit dislocations. The electrical activity after laser annealing is superior to that which can be achieved by thermal annealing, and there is no degradation of MCL in the substrate. Solar cells fabricated by using laser annealing of ion-implanted silicon have efficiencies almost 50 percent greater than those obtained by one-step thermal annealing, and the efficiencies obtained to date from unoptimized cells are only slightly lower than those obtained by the most sophisticated diffusion techniques.

Laser annealing should find wide application in many other areas of semiconductor technology. For example, the fabrication of deep junction devices may be facilitated because of the enhanced diffusion rates in liquid silicon. Laser annealing of compound semiconducting devices such as gallium-arsenide may be a viable method for avoiding decomposition of the semiconductor during annealing (*22, 38*). Localized annealing on a planar substrate is potentially a very important application, and significant results have been achieved with a 40-μm diameter beam from a *Q*-switched Nd:YAG laser (*21*). Laser annealing may also find application as a means for annealing ion-implanted polycrystalline materials that would avoid some of the problems associated with rapid diffusion along grain boundaries.

In the area of research on metals, the combination of ion implantation and laser annealing offers attractive possibilities for the formation of high-temperature superconductors, metastable superconductors, and metastable alloys. In general, laser annealing may find interesting applications in any processing step which requires rapid solidification or cooling at very high rates. Ion implantation followed by annealing with high-powered lasers may provide new ways for materials processing. The combination of these two existing technologies can be expected to yield significant results in the areas of materials modification and preparation of new materials.

References and Notes

1. See, for example, A. L. Robinson, *Science* **201**, 333 (1978) and H. R. Leuchtag, *Phys. Today* **31**, 17 (July 1978).
2. I. B. Khaibullin, E. I. Shtyrkov, M. M. Zaripov, M. F. Galyautdinov, G. G. Zakirov, *Sov. Phys. Semicond.* **11**, 190 (1977), and references therein.
3. A. Kh. Antonenko, N. N. Gerasimenko, A. V. Dvurechenskii, L. S. Smirnov, G. M. Tseitlin, *ibid.* **10**, 81 (1976), and references therein.
4. G. A. Kachurin, E. V. Nidaev, A. V. Khodyachikh, L. A. Kovaleva, *ibid.*, p. 1128.
5. R. T. Young, C. W. White, G. J. Clark, J. Narayan, W. H. Christie, in *Photovoltaic Solar Energy Conference, Proceedings of the International Conference, Luxembourg, September 27-30, 1977* (Reidel, Boston, 1978), p. 861.
6. ———, M. Murakami, P. W. King, S. D. Kramer, *Appl. Phys. Lett.* **32**, 139 (1978).
7. J. Narayan, R. T. Young, C. W. White, *J. Appl. Phys.* **49**, 3912 (1978).
8. ———, in *Proceedings of the Topical Conference on Characterization Techniques for Semiconductor Materials and Devices*, P. A. Barnes and G. A. Rozgonyi, Eds. (Electrochemical Society, New York, 1978), p. 473.
9. C. W. White, P. P. Pronko, S. R. Wilson, B. R. Appleton, J. Narayan, R. T. Young, *J. Appl. Phys.*, in press.
10. C. W. White, W. H. Christie, R. E. Eby, J. C. Wang, R. T. Young, G. J. Clark, R. F. Wood, in *Proceedings of the Topical Conference on Characterization Techniques for Semiconductor Materials and Devices*, P. A. Barnes and G. A. Rozgonyi, Eds. (Electrochemical Society, New York (1978), p. 482.
11. C. W. White, W. H. Christie, B. R. Appleton, S. R. Wilson, P. P. Pronko, C. W. Magee, *Appl. Phys. Lett.* **33**, 662 (1978).
12. J. C. Wang, R. F. Wood, P. P. Pronko, *ibid.*, p. 455.
13. B. C. Larson, C. W. White, B. R. Appleton, *ibid.* **32**, 801 (1978).
14. R. T. Young, C. W. White, J. Narayan, G. J. Clark, W. H. Christie, in *Proceedings of the Topical Conference on Characterization Techniques for Semiconductor Materials and Devices*, P. A. Barnes and G. A. Rozgonyi, Eds. (Electrochemical Society, New York, 1978), p. 466.
15. R. T. Young, C. W. White, J. Narayan, R. D. Westbrook, R. F. Wood, W. H. Christie, in *Proceedings of the 13th IEEE Photovoltaic Specialists Conference, 78-CH1319-3* (1978), p. 717.
16. R. T. Young and J. Narayan, *Appl. Phys. Lett.* **33**, 14 (1978).
17. ———, C. W. White, J. W. Cleland, W. H. Christie, R. F. Wood, in *Proceedings of the 13th IEEE Photovoltaic Specialists Conference, 78-CH1319-3* (1978), p. 1208.
18. J. Narayan, R. T. Young, R. F. Wood, W. H. Christie, *Appl. Phys. Lett.* **33**, 338 (1978).
19. C. W. White, J. Narayan, B. R. Appleton, S. R. Wilson, *J. Appl. Phys.*, in press.
20. W. L. Brown *et al.*, in *Proceedings of the Conference on Rapid Solidification Processing—Principles and Technologies, Reston, Va.* (Claitor's, Baton Rouge, La., 1978), p. 123.
21. G. K. Celler, J. M. Poate, L. C. Kimerling, *Appl. Phys. Lett.* **32**, 464 (1978).
22. J. A. Golovchenko and T. N. C. Venkatesan, *ibid.*, p. 147.
23. A. Gat, J. F. Gibbons, T. J. Magee, J. Peng, V. Deline, P. Williams, C. A. Evans, Jr., *ibid.*, p. 276.
24. G. Vitali, M. Bertolotti, G. Foti, E. Rimini, *Phys. Lett.* **63A**, 351 (1977).
25. S. U. Campisano, G. Ciavola, G. Vitali, *Appl. Phys.* **15**, 233 (1978).
26. G. Vitali, M. Bertolotti, G. Foti, E. Rimini, in *Proceedings of the Seventh International Conference on Amorphous and Liquid Semiconductors*, W. E. Spear, Ed. (Univ. of Edinburgh Press, Edinburgh, 1977), p. 24.
27. G. Foti, S. U. Campisano, E. Rimini, *J. Appl. Phys.* **49**, 2569 (1978).
28. P. Baeri, S. U. Campisano, G. Foti, E. Rimini, *Appl. Phys. Lett.* **33**, 137 (1978).
29. S. S. Lau, W. F. Tseng, M-A. Nicolet, J. W. Mayer, R. C. Eckardt, R. J. Wagner, *ibid.*, p. 130.
30. D. H. Auston, C. M. Surko, T. N. C. Venkatesan, R. E. Slusher, J. A. Golovchenko, *ibid.*, p. 437.
31. A. Gat, J. F. Gibbons, T. J. Magee, J. Peng, P. Williams, V. Deline, C. A. Evans, Jr., *ibid.*, p. 389.
32. J. S. Williams, W. L. Brown, H. J. Leamy, J. M. Poate, J. W. Rogers, D. Rousseau, G. A. Rozgonyi, J. A. Shelnutt, T. T. Sheng, *ibid.*, p. 542.
33. D. H. Auston, J. A. Golovchenko, P. R. Smith, C. M. Surko, T. N. C. Venkatesan, *ibid.*, p. 539.
34. H. Kodera, *Jpn. J. Appl. Phys.* **2**, 212 (1963).
35. A. S. Grove, in *Physics and Technology of Semiconductor Devices* (Wiley, New York, 1967), pp. 38, 39, and 45.
36. S. T. Picraux, in *New Uses of Ion Accelerators*, J. F. Ziegler, Ed. (Plenum, New York, 1975), p. 229.
37. M. S. Bae and R. V. D'Aiello, *Appl. Phys. Lett.* **31**, 285 (1977).
38. J. Narayan, C. W. White, R. T. Young, *Proceedings of the International Conference on Ion Beam Modification of Materials, Budapest, Hungary, September 1978*, in press.
39. Experimental results and theoretical calculations on projected ranges and range straggling for boron, phosphorus, and arsenic in silicon are summarized in D. H. Lee and J. W. Mayer, *Proc. IEEE* **62**, 1241 (1974).

40. The work summarized here is the result of collaboration with many of our colleagues at ORNL. In particular, we thank B. R. Appleton, W. H. Christie, G. J. Clark, B. C. Larson, P. P. Pronko, J. C. Wang, S. R. Wilson, R. F. Wood, and F. W. Young, Jr., for their participation. The research was sponsored by the Division of Materials Sciences, U.S. Department of Energy, under contract W-7405-eng-26 with the Union Carbide Corporation.